Materials Advances

ROYAL SOCIETY OF CHEMISTRY

PAPER

View Article Online
View Journal | View Issue

Cite this: *Mater. Adv.*, 2023, 4, 3619

Light and solvent-driven actuator of clay and vanadium pentoxide nanosheets†

Partha Pratim Saikia,‡[a] Priyanku Garg,‡[b] Kiran Mayawad,‡[b] Tumpa Paul,[cd] Arindom Bikash Neog,[be] Bhaskar Jyoti Sarmah,[f] Kalyan Raidongia [b] and Raj Kumar Gogoi §*[b]

Received 11th March 2023,
Accepted 13th July 2023

DOI: 10.1039/d3ma00119a

rsc.li/materials-advances

As the demand for advanced technological materials continues to rise, the lookout for materials capable of responding to external stimuli, such as heat, light, and chemical vapor, by changing their own shape and size is becoming increasingly important. Here, we report a novel light and vapor-responsive material prepared by a sequential assembly of exfoliated two-dimensional (2D) sheets of vermiculite and vanadium pentoxide (V_2O_5). Nanosheets of V_2O_5 are prepared by treating bulk V_2O_5 powder with H_2O_2 and those of vermiculite are obtained by stirring the bulk crystals in an HCl solution. The bilayer membrane of V_2O_5 and vermiculite displays outstanding shape-morphing characteristics upon exposure to light. The infrared light (IR) induced higher bending and recovery speeds (20.5° s^{-1} and 8.2° s^{-1}) as compared to the white light (9.3° s^{-1} and 6.4° s^{-1}). Unequal changes to the mechanical properties at the two sides of the bilayer membrane due to dissimilar light-induced heating are attributed to the shape-morphing characteristics. The light-induced bending movement of this bilayer membrane is also utilized to translocate objects from one place to another. Additionally, the bilayer membrane also responds to the presence of solvent vapors like 2-propanol, ethanol, methanol, ethyl acetate, dichloromethane (DCM), and acetone vapor by morphing its shape in a specific manner.

1. Introduction

The development of materials responding to minute changes in their surrounding environments like heat,[1,2] light,[1,3–5] humidity,[6–8] liquids,[9,10] and chemical vapor[7,11–13] by changing their characteristics like size,[14] shapes,[2,7,11,12] and color[15,16] is considered a matter of great importance in advanced technologies. To facilitate fast, accurate, and specific responsiveness in artificially intelligent systems such as artificial muscles, soft robots, actuators, and programmable devices, researchers are working on developing responsive materials with explicit characteristics tailored to specific applications.[17–22] Among these materials, light-driven actuators are particularly significant due to their potential for futuristic engineering applications, such as contactless operations, remote activation, and targeted response.[23] Moreover, as a clean and sustainable stimulus, light offers tremendous flexibility and convenience in performing complicated tasks contact-free.

Taking into account their potential for numerous futuristic applications, light-responsive materials were prepared using different nanomaterials, polymers, and even nano-composites. For example, Liu *et al.* developed a high-efficiency actuator with great photo-induced force through gradient design of the components, silver nanowires in poly(ethylene-*co*-vinyl acetate) elastomers.[19] A photo-thermal Marangoni-driven triboelectric nano-generator was designed by Liu *et al.* by utilizing black silicon to propel relative motions between the triboelectric layer and the electrode.[24] An integrated multi-functional light-driven actuator with temperature sensitivity was designed by Xiao *et al.* using carbon nanotubes (CNTs) and a methylcellulose nano-composite.[25] A light-responsive superhydrophobic film exhibiting a bending angle above 200° was fabricated by sequentially dip coating a carbon nanotubes/poly(vinylidene fluoride) composite layer and a chitosan layer, followed by spraying fumed silica-chitosan composite and modification with 1*H*,1*H*,2*H*,2*H*-heptafluorodecyltrimethoxysilane.[26] A core-shell fibre-shaped

[a] *Department of Chemistry, Nanda Nath Saikia College, Titabar-785630, Assam, India*
[b] *Department of Chemistry, Indian Institute of Technology Guwahati, Guwahati, 781039, Assam, India. E-mail: raj.gogoi@alumni.iitg.ac.in*
[c] *Department of Chemistry, Darrang College, Tezpur-784001, Assam, India*
[d] *Assam Science and Technology University, Guwahati-781013, Assam, India*
[e] *Department of Chemistry, Dergaon Kamal Dowerah College, Golaghat-785614, Assam, India*
[f] *Department of Chemistry, Jorhat Institute of Science and Technology, Jorhat-785010, Assam, India*

† Electronic supplementary information (ESI) available. See DOI: https://doi.org/10.1039/d3ma00119a

‡ These authors contributed equally.

§ Present address: Department of Physics & Astronomy, University of Manchester, Manchester, M13 9PL, U.K.

soft actuator that can lift loads more than 4600 times its weight was prepared by coating liquid crystal elastomer on a CNT shell.[27] Along with these, several recently published articles demonstrate significant progress in fabrication methods, novel functionalities and diverse application possibilities. However, preparing all these light-responsive materials requires exotic materials and sophisticated laboratory facilities, which hinders their practicality. On the other hand, multiple highly responsive and robust smart materials were prepared by re-stacking exfoliated flakes of two or more different layered materials.[11,12,28,29] The synthesis and assembly of exfoliated 2D layers is a straightforward and scalable process, and therefore intelligent materials prepared by the reconstruction of 2D materials possess enormous potential for practical applications. Graphene oxide (GO) is one of the most well-studied exfoliated 2D materials due to its exclusive properties and scalable synthesis process. It has found applicability in numerous areas, including catalysis, supercapacitors, batteries, nanofluidics, and water purification.[30–35] The relevant literature indicates that GO membranes' reconstructed layers are an excellent component of bilayer-based responsive materials. For example, bilayers of GO and reduced-GO were found to be highly responsive to changes in humidity and electric field.[29] Similarly, bilayers of multi-walled CNTs and GO demonstrated responsiveness towards humidity and temperature.[36] Bilayers of clay and GO showed outstanding sensitivity toward the vapors of solvent molecules such as methanol, ethanol, isopropanol, tetrahydrofuran, ethyl acetate, DCM, acetone, and water.[12]

The reconstructed membrane of vanadium pentoxide (VO-M) is emerging as an outstanding material for diverse applications. Due to the ease of exfoliation and excellent dispersibility of V_2O_5

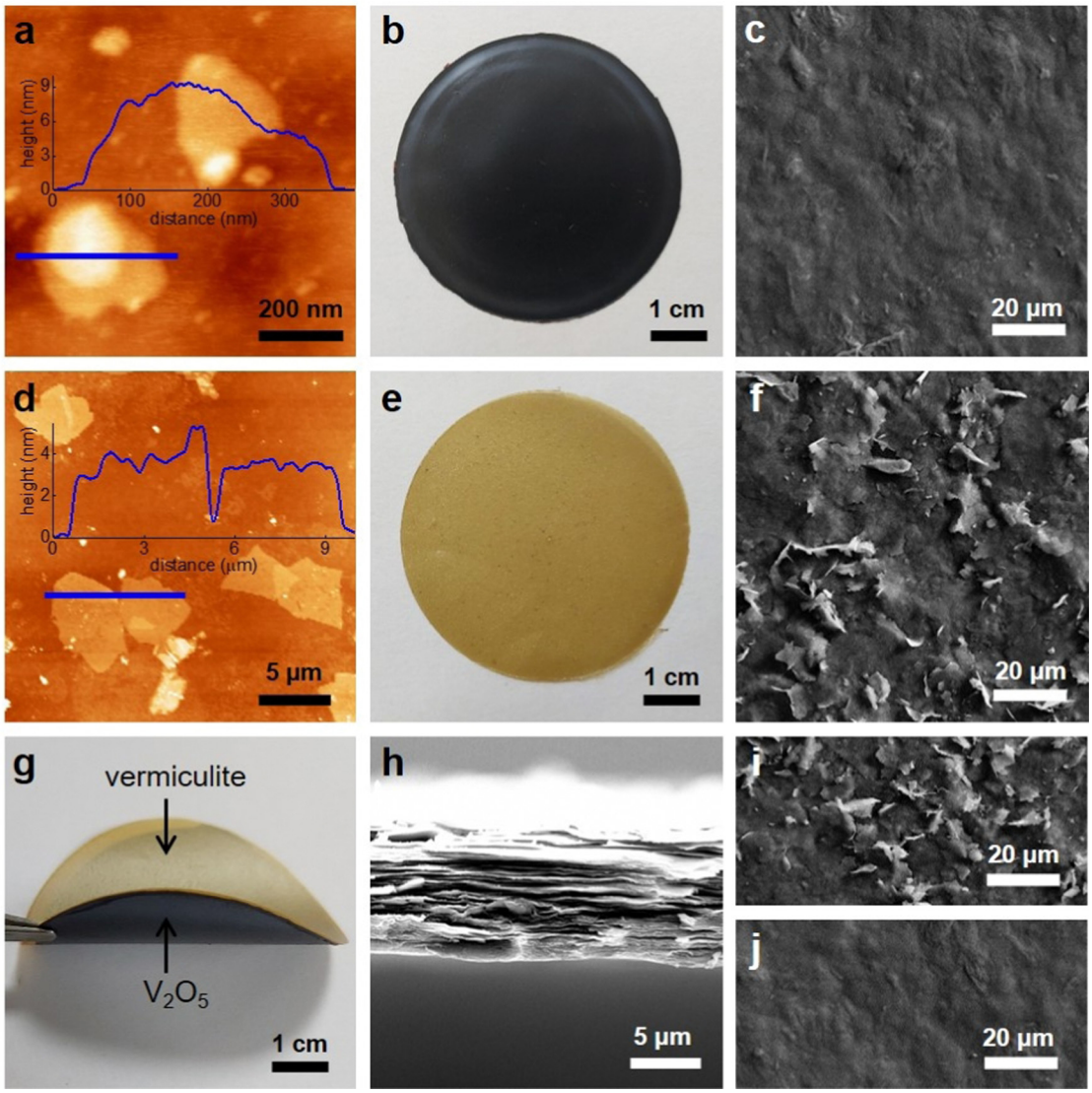

Fig. 1 Reconstructed V_2O_5-vermiculite bilayer membrane: AFM images with the corresponding height profiles of (a) V_2O_5 and (d) vermiculite 2D nanosheets. Photos of reconstructed (b) VO-M, (e) vermiculite and (g) V_2O_5-vermiculite membranes. FESEM images of the surfaces of (c) V_2O_5 and (f) vermiculite membranes. FESEM images of the (h) cross-section, (i) vermiculite and (j) V_2O_5 sides of the bilayer membrane.

flakes in an aqueous medium, the fabrication of VO-M is a highly scalable process.[37,38] The applicability of VO-M is also supported by the natural abundance and outstanding chemical and thermal stability of V_2O_5.[39–41] Considering its high surface charge density and moisture-sensitive properties,[37] VO-M could be an excellent ingredient for preparing intelligent materials. However, in contrast to GO, VO-M has not been explored much for preparing responsive materials, except for the effort of Gogoi *et al.*, where macroscopic bilayer membranes were prepared by self-assembling nanosheets and nanobelts of V_2O_5.[42] The morphology-based bilayer membranes of V_2O_5 responded to multiple environmental stimuli such as solvent vapor, humidity, and light by changing their shape. Here, we reconstructed a bilayer membrane of V_2O_5 and vermiculite nanosheets, decorated with stimuli-responsiveness. The mechanical moment of this bilayer membrane has been utilized to translocate objects through rational designing. The natural abundance of the raw materials in combination with the straightforward and trouble-free fabrication methods for the synthesis and assembly of the V_2O_5 and vermiculite nanosheets with rational design will pose no practical limitation for real-field applications.

2. Results and discussion

2D nanosheets of V_2O_5 were restacked on exfoliated vermiculite clay to prepare a multi-responsive actuator by self-assembling individual nanosheets from their respective dispersions. The V_2O_5 nanosheets were prepared by the reaction of the bulk V_2O_5 powder with H_2O_2 in an aqueous medium.[37,38] The composition of the nanosheets as V_2O_5 was confirmed by XPS analysis, Fig. S2 (ESI†). A representative atomic force microscopy (AFM) image of the V_2O_5 nanosheets (Fig. 1a) reveals the height and lateral dimensions of the nanosheets to be in the range of $\sim$9 nm and $\sim$300 nm, respectively. The vacuum filtration of the aqueous dispersion of the V_2O_5 nanosheets (Fig. S1, ESI†) through polytetrafluoroethylene (PTFE) filter paper forms a flexible and free-standing membrane (Fig. 1b), with a lamellar structure (confirmed by the presence of the 001 plane in the XRD spectra, Fig. S8a, ESI†) and a smooth outher surface (field emission scanning electron microscopy (FESEM) image in Fig. 1c). The vermiculite section of the bilayer was prepared by exfoliating the bulk crystals of vermiculite (Fig. S3a, ESI†) into 2D layers by stirring it in a dilute HCl solution for around 18 hours.[12] The representative AFM image in Fig. 1d shows that the average lateral dimensions of the 2D sheets are $\sim 5 \times 4\ \mu m^2$ with a thickness of $\sim$3.5 nm. These exfoliated 2D vermiculite layers from a stable dispersion in deionized (DI) water, Fig. S3b (ESI†). Like the V_2O_5, vermiculite also forms a flexible and free-standing membrane, Fig. 1e. The outer surface of the vermiculite membranes is shown in the FESEM image in Fig. 1f. To prepare the V_2O_5-vermiculite bilayer actuator, first, the aqueous dispersion of vermiculite nanosheets (12 mL of 1 mg mL^{-1}) was vacuum filtered through PTFE filter paper. Once the vermiculite membrane formed, 6 mL of 3 mg mL^{-1} V_2O_5 nanosheet dispersion was filtered through it. The bilayer membrane, composed of vermiculite on one side and V_2O_5 nanosheets on the other side, was detached from the filter paper upon complete drying and the thickness is measured to be 15 μm. The two sides of the bilayer can be easily distinguished from the color grey-black for the V_2O_5 and yellow-brown for the vermiculite side, Fig. 1g. In the bilayer membrane the interface between the vermiculite and V_2O_5 is indistinguishable, see the cross-sectional FESEM image in Fig. 1h. This is because both the vermiculite and VO-M consist of 2D nanosheets. However, the outer surface of the vermiculite side has a rough morphology (Fig. 1i) as compared to that of the VO-M surface (Fig. 1j). The thickness of the vermiculite and V_2O_5 portions in the bilayer membrane can be easily controlled by the volume and the concentrations of the individual nanosheet dispersions used to prepare the bilayer (discussed in table S1, ESI†). Thus, for the 15 μm thick bilayer membrane, the vermiculite and V_2O_5 sections were measured to have a thickness of 6 μm and 9 μm, respectively.

The light-induced responsiveness of the bilayer actuator was investigated by exposing it to different light sources and recording the shape-morphing moments using a digital camera. A rectangular strip (length = 25 mm and width = 2 mm) was tailor-cut from the bilayer membrane (thickness = 15 μm) and fixed to a rod with one end, leaving the other end to move freely (Fig. S4, ESI†). Exposing the strip to IR light (150 W, 4000 lux), we observed the strip bending towards the V_2O_5 side, and it regained its original configuration after removing the light source (shown in Fig. 2a and Video V1, ESI†). This IR-light-induced shape-morphing characteristic of the bilayer membrane was found to be highly reversible. However, the individual membranes, *i.e.*, vermiculite and VO-M, did not exhibit any light-induced shape-changing properties. Moreover, this bilayer strip also demonstrates similar shape-changing characteristics when exposed to white light (1000 W, 50 000 lux); snapshots are shown in Fig. 2b (and Video V2, ESI†). The bending angle (quantification strategy is in Fig. S5, ESI†) exhibited by the bilayer strip was quantified and plotted as a function of time in Fig. 2c. Remarkably, even though the power of the white light is 12.5 more than the IR light, the IR light induced a higher bending angle (bent by 80°) than that of the white light (bent by 70°). The bending and recovery speeds of the bilayer strip were estimated by analyzing the recorded video. It was observed that the IR light induced higher bending and recovery speeds (20.5° s^{-1} and 8.2° s^{-1}, respectively) as compared to the white light (9.3° s^{-1} and 6.4° s^{-1}, respectively), see Fig. 2d.

The shape of the bilayer actuators where two different layers are fused into a thin film is determined by the equilibrium of the mechanical properties of the individual components forming the actuator. Any dissimilar variations in the mechanical properties of the individual components shift the equilibrium into a new position resulting in shape transformation.[7,11,12] To understand the mechanism of the light-induced responsiveness of the bilayer membrane, we recorded the photo-thermal images of the individual membranes in the presence and

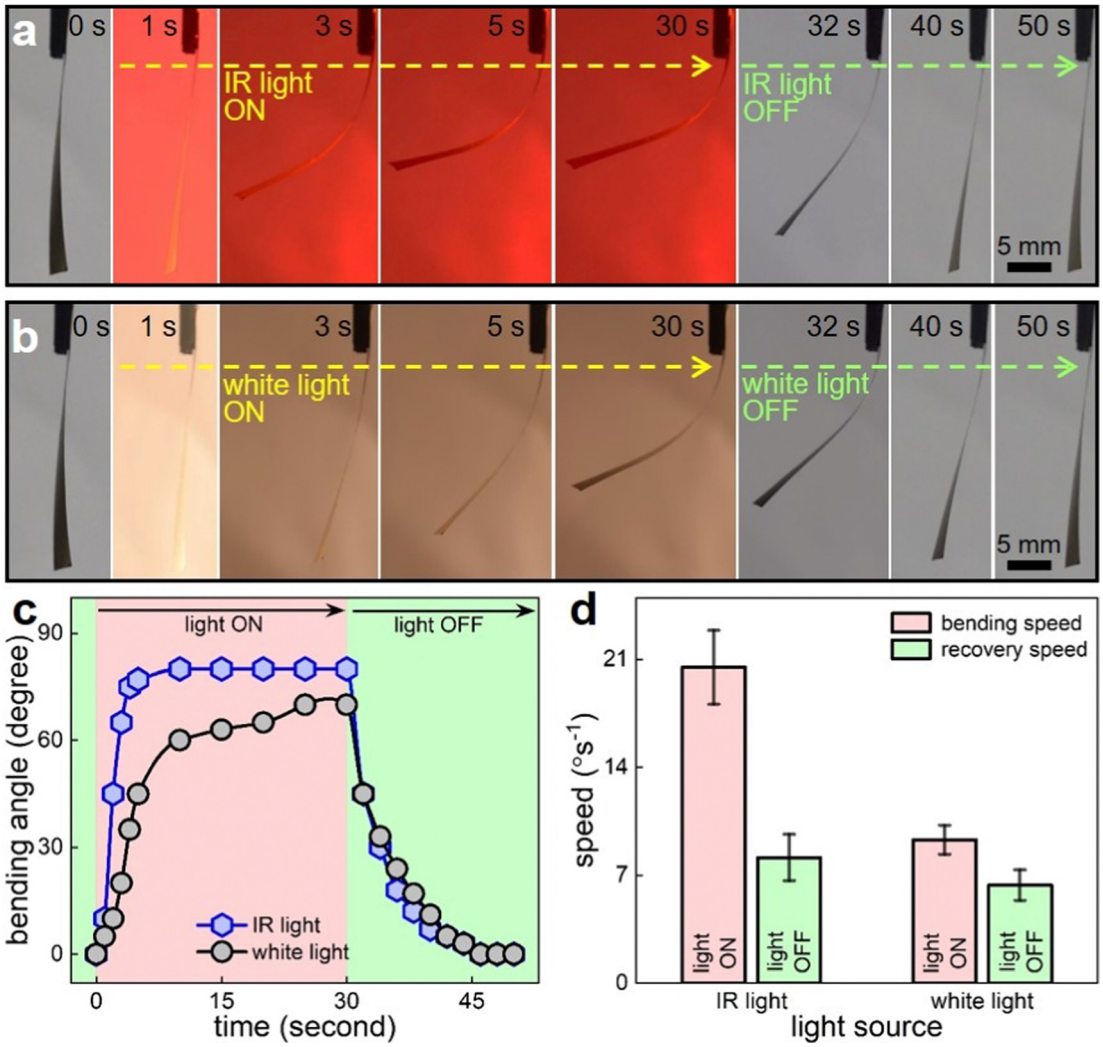

Fig. 2 Light-induced responsiveness of the reconstructed V_2O_5-vermiculite bilayer actuator: Snapshots showing the bending and recovery moments of a bilayer strip (25 mm × 2 mm, thickness 15 μm) upon exposure to (a) IR and (b) white light. (c) Plots comparing the bending angle of a bilayer strip in the presence and absence of the light sources. (d) Bar diagram comparing a bilayer strip's bending and recovery speeds upon exposure to IR and white light. The error bars in (d) are calculated from different experiments of five different strips having similar composition and dimensions.

absence of the light sources (Fig. 3a and b, left and middle images for the presence and absence of the IR light). Upon exposure to IR light, the temperature of the VO-M increased by 29 °C, whereas that of vermiculite increased by 10 °C, Fig. 3c. Thus, these dissimilar heatings at the two sides of the bilayer membrane will induce unequal changes to the mechanical properties resulting in shifting the equilibrium and hence inducing the shape transformation. Further insight into the mechanism was achieved by measuring the change in the water content of the individual membranes upon IR light exposure, Fig. S6 (ESI†). The relative humidity (RH) of the VO-M decreased by 17% whereas it is 3.5% for the vermiculite membrane, Fig. S6c (ESI†). This suggests that the V_2O_5 side contracted more than the vermiculite side due to the higher loss of water molecules and bent towards the V_2O_5 side. Similar experimental studies were also performed for both membranes upon exposure to white light. But, the increase in the temperature of the VO-M is 16 °C, and that of vermiculite is 11 °C (Fig. 3c); hence, white light induced lower bending speed in comparison to the IR light. In addition, the IR (Fig. S7, ESI†) and the XRD (Fig. S8, ESI†) spectra of the VO-M and the vermiculite membranes are recorded before and after exposure to IR light and no significant changes were observed in the membranes.

As the irradiation of light induced a temperature increase to the actuator, it is essential to investigate the thermal stability. Strips of the V_2O_5-vermiculite actuator were heated up to 100 °C for 30 minutes in an air atmosphere and thereafter cooled down to room temperature. The bilayer strips form coiled-like shapes upon heating, which regained the original configuration after cooling, which is highly reversible (Fig. S9a, ESI†). The high thermal stability of the bilayer actuator is inherited from the excellent thermal stability of the individual components, *i.e.*, vermiculite and V_2O_5. The weight loss graphs of the

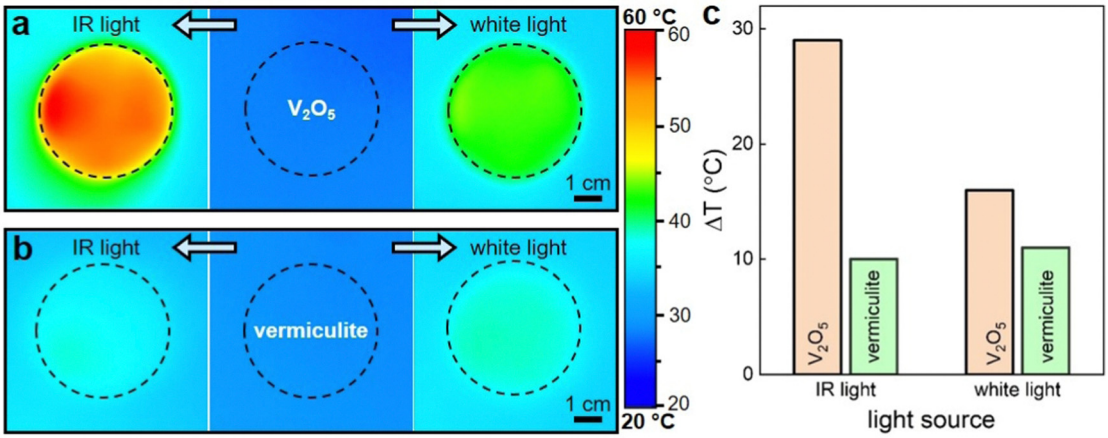

Fig. 3 Mechanism of light-induced responsiveness: Photothermal images showing the heating of individual (a) VO-M and (b) vermiculite membranes upon exposure to IR light (left side) and white light (right side). (c) Bar diagram comparing the change in temperature (ΔT) of V_2O_5 and vermiculite membranes upon exposure to light sources.

VO-M, vermiculite and V_2O_5-vermiculite bilayer membranes upon heating are compared in Fig. S9b (ESI†). During heating, it was observed that the actuator bent towards the V_2O_5 side. To gain further insight, we estimated the rate of weight loss of the individual membranes and found that VO-M exhibits a higher rate of weight loss (0.06% per °C) than that of vermiculite (0.04% per °C); hence, the actuator bent towards the V_2O_5 side. This weight loss of the membranes can be attributed to the loss of water from the interlayer spacing.

The light-induced bending moment of this bilayer membrane can be utilized to translocate objects from one place to another. As a proof of concept, we made a cantilever from two bilayer strips (dimensions, 25 mm × 2 mm, thickness of 15 μm) by placing them perpendicularly and fixed to a rod. Exposing it to a light source, the arms bent inward and recovered with the removal of the light source. We now utilize this cantilever to translocate objects from one place to another, shown in Fig. 4a and Video V3 (ESI†). Furthermore, we have also demonstrated

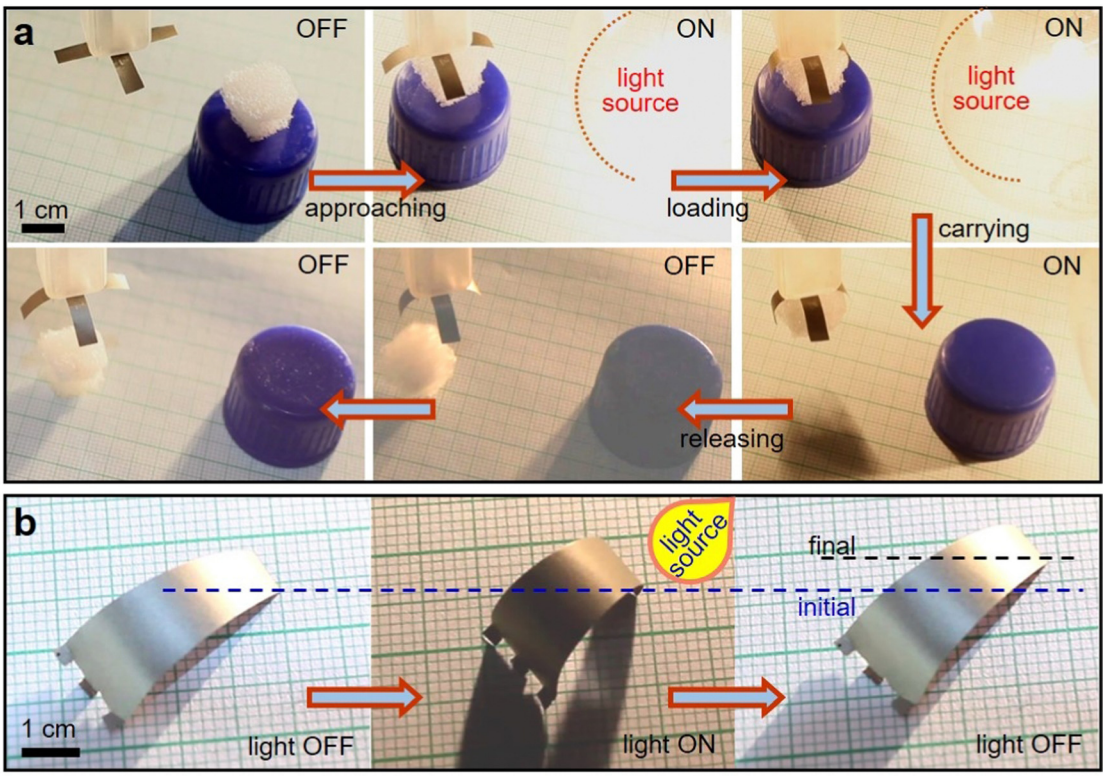

Fig. 4 Light-induced actuation: (a) Photos showing the translocation of an object and (b) worm-like walking (speed ~0.7 mm s^{-1}) of the V_2O_5-vermiculite bilayer actuator. (Light ON and light OFF refer to the white light, 1000 W, 50 000 lux.)

the worm-like walking of the bilayer membrane. We cut a trapezoidal strip from the membrane (length = 25 mm, base = 8 mm and tip = 4 mm, Fig. S10, ESI†), which walks like a worm with a speed of $\sim$ 0.7 mm s^{-1} upon periodic exposure to a light source (Video V4, ESI† and Fig. 4b). The walking of the strip is due to it's bending in the presence of light and tends to retain the original shape in the absence. This type of actuation of the bilayer membrane can be utilized to perform tasks where human presence is not preferred.

In addition, the bilayer membrane also responded to the presence of solvent vapor in its surrounding environment. Upon exposure to the 2-propanol vapor (maintaining a distance of 15 mm between the strip and the solvent surface, see experiment set-up, Fig. S11, ESI†) the strip responded to the change in its surrounding by bending toward the vermiculite side with a bending speed of 12.3° s^{-1} until it attained a fixed configuration and remained at that configuration with further exposure. The strip retained the original configuration with a recovery speed of 13° s^{-1} after removing the 2-propanol environment (Video and snapshots are shown in Video V5, ESI† and Fig. 5a, respectively). The influence of the distance between the solvent surface and the bilayer strip (dimensions, 25 mm × 2 mm × 15 μm) was studied by increasing the distance from 15 mm to 60 mm upon exposure to 2-propanol vapours. The maximum bending angle decreased from 165° to 48° on increasing the distance from 15 mm to 60 mm, Fig. 5b. Furthermore, we investigated the effect of the thickness of the bilayer membrane on the responsiveness by making three bilayers of thickness 15 μm (vermiculite = 6 μm, and V_2O_5 = 9 μm), 22 μm

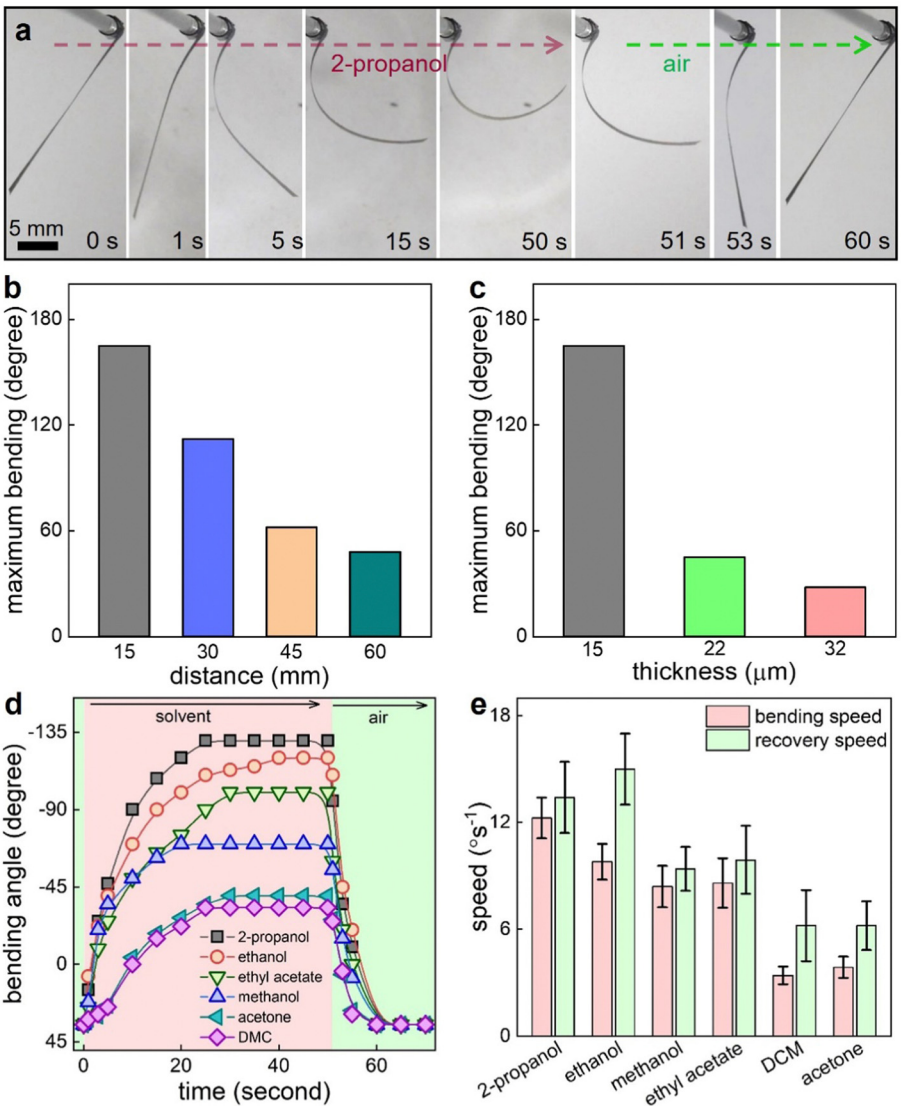

Fig. 5 Solvent-induced responsiveness: (a) Snapshots showing the bending and the recovery moment of the V_2O_5-vermiculite bilayer strip upon exposure to 2-propanol vapor. Bar diagram comparing the maximum bending angle as a function of (b) the distance between the strip and the solvent surface and (c) the thickness of the bilayer membranes in the presence of 2-propanol vapours. In (c) the distance between the solvent and the strip is 15 mm, and the length and width of the strips are 25 mm and 2 mm, respectively. (d) Comparison of the bending angle and (e) the bending and the recovery speeds of the bilayer strips in the presence of solvent vapor. The error bars in (e) are calculated from different experiments of five different strips having similar composition and dimensions. In (a), (b), (d) and (e), the length, width and thickness of the strips are 25 mm, 2 mm and 15 μm, respectively.

(vermiculite = 9 μm, and V_2O_5 = 13 μm), and 32 μm (vermiculite = 13 μm, and V_2O_5 = 19 μm) (see Table S1, ESI†). The increase in thickness of the membrane from 15 to 32 μm decreased the extent of bending from ~165° to ~28° when exposed to 2-propanol vapours, Fig. 5c.

This solvent-induced responsiveness of the bilayer strip was found to be highly reversible. This bilayer strip was also responsive towards ethanol, methanol, ethyl acetate, DCM, and acetone vapor and responded to them by bending toward the vermiculite side (Fig. S12, ESI†). The changes in the shape in terms of the bending angle of the strip to different vapors are compared Fig. 5d. Moreover, the strip responded to these vapors with different bending and recovery speeds, Fig. 5e. However, solvents like benzene, chloroform and toluene did not induce any physical changes to the actuator (Fig. S13, ESI†).

As the V_2O_5-vermiculite bilayer actuator results from the fusion of two thin films, we studied the effect of solvent vapor on the mechanical properties of the individual components forming the actuator to understand the mechanism of solvent vapor-induced responsiveness. The bending stiffness (S_B), which represents the resistance to bending, of the individual VO-M and vermiculite membranes, was measured using the Lorentzen & Wettre two-point method, both in the absence and presence of the solvent vapor.[11,43] In the presence of 2-propanol vapor, the S_B of the VO-M decreased by 43%, but no significant change was observed for the vermiculite membrane (Fig. 6b). This unparallel change in the S_B of individual layers triggered the shape transformation in the bilayer actuator by bending towards the vermiculite. Moreover, we record the change in the S_B of the individual membranes when exposed to ethanol and methanol vapor. Similar to the 2-propanol exposure, the S_B for the VO-M also decreased in the presence of ethanol and methanol, but with a different magnitude (Fig. 6b). In contrast, no significant change was observed for the vermiculite part in the presence of these vapors (Fig. 6b). The change in the S_B of the individual components depends on molecules/desorption of the interlayer water/solvent molecules and hence, the specific bending angle of the actuator to the presence of stimuli at any particular time is attributed to the equilibrium between the mechanical properties of the individual components forming the membrane. This implies that the V_2O_5 portion plays an active role in the shape transformation with the vermiculite as the supporting layer, and the extent of the bending is proportional to the decrease in the S_B of the VO-M. Among the 2-propanol,

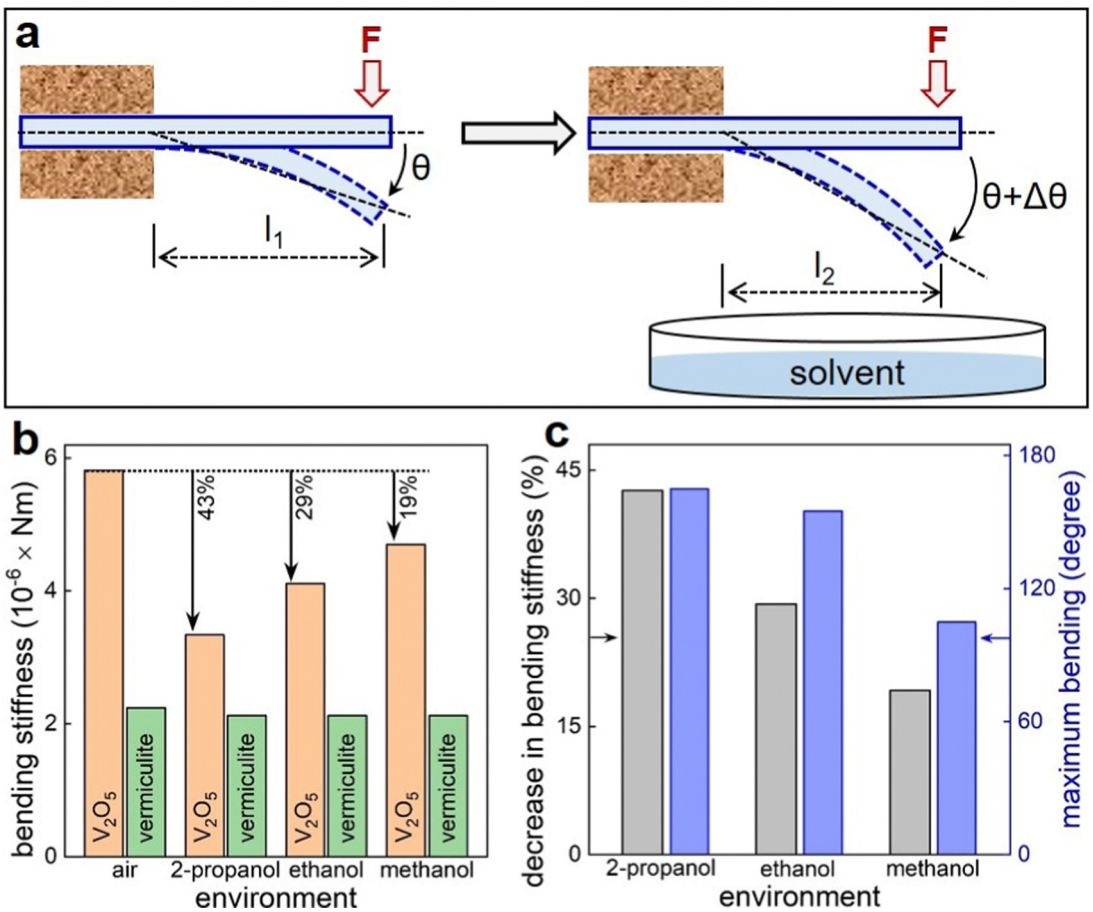

Fig. 6 Mechanism of solvent-induced responsiveness: (a) Schematic illustration of bending stiffness measurement using Lorentzen & Wettre's two-point method. Bar diagrams comparing (b) the bending stiffness of VO-M and vermiculite membranes upon exposure to different environments and (c) the decrease in bending stiffness (in %) of the V_2O_5 strip with the extent of bending for the bilayer actuator in the presence of solvent vapor.

ethanol and methanol, the decreases in S_B (ΔS_B) for the VO-M are in the order: ΔS_B (2-propanol) > ΔS_B (ethanol) > ΔS_B (methanol) and the extent of bending (θ) of the actuator is in the order: $\theta_{2\text{-propanol}} > \theta_{\text{ethanol}} > \theta_{\text{methanol}}$ (Fig. 6c).

3. Conclusion

In conclusion, we demonstrated the fabrication of new responsive materials through sequential deposition of aqueous dispersions of 2D flakes of V_2O_5 and vermiculite. The bilayer membranes of V_2O_5 and vermiculite have shown outstanding responsiveness towards light and solvent vapors. Unequal changes in the mechanical properties at the two sides of the bilayer membrane are attributed to the shape-morphing characteristics. Dissimilar light-induced heating and reversible absorption-desorption characteristics of vapour molecules from the interlayer space of the components accounted for the inequality in the changes of the mechanical properties. As IR light-induced a higher rise in temperature of V_2O_5 as compared to that of white light, it yielded higher bending speeds. The light-induced bending movement of this bilayer membrane can be applied for different applications like remote handling/transportation of objects from one place to another. The bilayer membrane also senses the presence of a large number of solvent vapors like isopropanol, ethanol, methanol, ethyl acetate, DCM, and acetone vapor and responds by morphing its shape in a specific manner. The responsiveness and sensitivity of the V_2O_5–vermiculite bilayer membrane can be further improved through various possible modes of functionalization, which would offer many enthusing opportunities for novel applications. The V_2O_5–vermiculite bilayer membranes could also be applied for sensing chemical vapor and harvesting light energy.

Conflicts of interest

The authors declare no competing financial interests.

Acknowledgements

The authors would like to acknowledge the SERB, India, for financial support (project number CRG/2020/002943), the CIF and NECBH of IITG for sample characterizations. P. P. S. thanks SERB (project number TAR/2021/000132) for the fellowship. K. M. is grateful for the PMRF fellowship. R. K. G. and A. B. N. are grateful to IITG for PhD fellowships.

References

1 F. D. Jochum and P. Theato, *Chem. Soc. Rev.*, 2013, **42**, 7468–7483.
2 C. Wang, Y. Wang, Y. Yao, W. Luo, J. Wan, J. Dai, E. Hitz, K. Fu and L. Hu, *Adv. Mater.*, 2016, **28**, 8618–8624.
3 X. Zhang, Z. Yu, C. Wang, D. Zarrouk, J.-W. T. Seo, J. C. Cheng, A. D. Buchan, K. Takei, Y. Zhao, J. W. Ager, J. Zhang, M. Hettick, M. C. Hersam, A. P. Pisano, R. S. Fearing and A. Javey, *Nat. Commun.*, 2014, **5**, 2983.
4 B. Li, Y. Zhang, T. Li, H. Yu, Q. Guo, M. Hu and J. Yang, *Macromol. Mater. Eng.*, 2022, **307**, 2100868.
5 Z. Su, Y. Zhao, Y. Huang, C. Xu, X. Yang, B. Wang, B. Xu, S. Xu and G. Bai, *Nano Res.*, 2023, **16**, 1313–1319.
6 L. Zhang, H. Liang, J. Jacob and P. Naumov, *Nat. Commun.*, 2015, **6**, 7429.
7 Q. Zhao, J. W. C. Dunlop, X. Qiu, F. Huang, Z. Zhang, J. Heyda, J. Dzubiella, M. Antonietti and J. Yuan, *Nat. Commun.*, 2014, **5**, 4293.
8 J. Li, M. Wang, Z. Cui, S. Liu, D. Feng, G. Mei, R. Zhang, B. An, D. Qian, X. Zhou and Z. Liu, *J. Mater. Chem. A*, 2022, **10**, 25337–25346.
9 M. Wang, L. Zhou, W. Deng, Y. Hou, W. He, L. Yu, H. Sun, L. Ren and X. Hou, *ACS Nano*, 2022, **16**, 2672–2681.
10 A. B. Neog, R. K. Gogoi, P. Deka, T. J. Konch, B. R. Bora and K. Raidongia, *New J. Chem.*, 2021, **45**, 16883–16891.
11 R. K. Gogoi and K. Raidongia, *Adv. Mater.*, 2017, **29**, 1701164.
12 R. K. Gogoi, K. Saha, J. Deka, D. Brahma and K. Raidongia, *J. Mater. Chem. A*, 2017, **5**, 3523–3533.
13 R. K. Gogoi and K. Raidongia, *J. Mater. Chem. A*, 2018, **6**, 21990–21998.
14 N. Zhang, R. Li, L. Zhang, H. Chen, W. Wang, Y. Liu, T. Wu, X. Wang, W. Wang, Y. Li, Y. Zhao and J. Gao, *Soft Matter*, 2011, **7**, 7231–7239.
15 Y. Shi, C. Zhu, J. Li, J. Wei and J. Guo, *New J. Chem.*, 2016, **40**, 7311–7319.
16 J. Peng, Y. Cheng, A. P. Tomsia, L. Jiang and Q. Cheng, *ACS Appl. Mater. Interfaces*, 2017, **9**, 24993–24998.
17 L. Li, G. Jia, W. Huang, J. Zhou, C. Li, J. Han, Y. Zhang and X. Zhou, *Sens. Actuators, A*, 2023, **351**, 114149.
18 D. Xiao, M.-T. Zheng and F.-J. Wu, *Chem. Eng. J.*, 2023, **459**, 141546.
19 M. Liu, Z. Xu, Y. Lv, S. Zhu, W. Liu, L. Yang and D. Ge, *J. Mater. Chem. C*, 2022, **10**, 8931–8937.
20 J. Laws and R. Parachuru, *Review*, 2021, **10**, 5–10.
21 A. Zhang, F. Wang, L. Chen, X. Wei, M. Xue, F. Yang and S. Jiang, *Chin. Chem. Lett.*, 2021, **32**, 2923–2932.
22 A. B. Neog, R. K. Gogoi, T. Dutta and K. Raidongia, *ACS Appl. Nano Mater.*, 2020, **3**, 6629–6635.
23 Y. Yu, M. Nakano and T. Ikeda, *Nature*, 2003, **425**, 145.
24 C. Liu, D. Jiang, G. Zhu, Z. Li, X. Zhang, P. Tian, D. Wang, E. Wang, H. Ouyang, M. Xiao and Z. Li, *ACS Appl. Mater. Interfaces*, 2022, **14**, 22206–22215.
25 Y. Xiao, J. Lin, J. Xiao, M. Weng, W. Zhang, P. Zhou, Z. Luo and L. Chen, *Nanoscale*, 2021, **13**, 6259–6265.
26 L. Zheng, H. Li, W. Huang, X. Lai and X. Zeng, *ACS Appl. Mater. Interfaces*, 2021, **13**, 36621–36631.
27 Y. Yu, L. Li, E. Liu, X. Han, J. Wang, Y.-X. Xie and C. Lu, *Carbon*, 2022, **187**, 97–107.
28 K. Saha, J. Deka, R. K. Gogoi, K. K. R. Datta and K. Raidongia, *ACS Appl. Nano Mater.*, 2022, **5**, 15972–15999.

29 H. Bi, K. Yin, X. Xie, Y. Zhou, S. Wan, F. Banhart and L. Sun, *Nanoscale*, 2013, **5**, 9123–9128.
30 A. Nag, A. Mitra and S. C. Mukhopadhyay, *Sens. Actuators, A*, 2018, **270**, 177–194.
31 D. A. Dikin, S. Stankovich, E. J. Zimney, R. D. Piner, G. H. B. Dommett, G. Evmenenko, S. T. Nguyen and R. S. Ruoff, *Nature*, 2007, **448**, 457–460.
32 J. Gao, Y. Feng, W. Guo and L. Jiang, *Chem. Soc. Rev.*, 2017, **46**, 5400–5424.
33 D. C. Elias, R. R. Nair, T. M. G. Mohiuddin, S. V. Morozov, P. Blake, M. P. Halsall, A. C. Ferrari, D. W. Boukhvalov, M. I. Katsnelson, A. K. Geim and K. S. Novoselov, *Science*, 2009, **323**, 610–613.
34 J. Abraham, K. S. Vasu, C. D. Williams, K. Gopinadhan, Y. Su, C. T. Cherian, J. Dix, E. Prestat, S. J. Haigh, I. V. Grigorieva, P. Carbone, A. K. Geim and R. R. Nair, *Nat. Nanotechnol.*, 2017, **12**, 546–550.
35 R. K. Joshi, P. Carbone, F. C. Wang, V. G. Kravets, Y. Su, I. V. Grigorieva, H. A. Wu, A. K. Geim and R. R. Nair, *Science*, 2014, **343**, 752–754.
36 S. Park, J. An, J. W. Suk and R. S. Ruoff, *Small*, 2010, **6**, 210–212.
37 R. K. Gogoi, A. B. Neog, T. J. Konch, N. Sarmah and K. Raidongia, *J. Mater. Chem. A*, 2019, **7**, 10552–10560.
38 Y. Li, C. Liu, Z. Xie, J. Yao and G. Cao, *J. Mater. Chem. A*, 2017, **5**, 16590–16594.
39 J. Mei, T. Liao, L. Kou and Z. Sun, *Adv. Mater.*, 2017, **29**, 1700176.
40 S. Beke, *Thin Solid Films*, 2011, **519**, 1761–1771.
41 R. B. Darling and S. Iwanaga, *Sadhana*, 2009, **34**, 531–542.
42 R. K. Gogoi, A. B. Neog, N. Sarmah and K. Raidongia, *J. Mater. Chem. A*, 2019, **7**, 21157–21167.
43 R. E. Mark, C. C. Habeger, J. Borch and M. B. Lyen, *Handbook of Physical Testing of Paper*, 2001, vol. 1.